https://doi.org/10.1016/j.ceramint.2020.04.157

Synthesis and characterization of Sb-doped SnO_2 with high near-infrared shielding property for energy-efficient windows by a facile dual-titration co-precipitation method

Boxu Shen[1], Yuanhao Wang[1,2,], Lin Lu[1], Hongxing Yang[1,*]*

1. Renewable Energy Research Group (RERG), Department of Building Services Engineering, The Hong Kong Polytechnic University, Kowloon, Hong Kong

2. Hoffmann Institute of Advanced Materials, Shenzhen Polytechnic, Shenzhen, China

*Corresponding author: Yuanhao Wang; Hongxing Yang

E-mail addresses: yuanhaowang@yahoo.com, wangyuanhao@szpt.edu.cn (Y. Wang);

hong-xing.yang@polyu.edu.hk (H. Yang)

Tel./Fax numbers: +86 13826520347 (Y. Wang); +852 2766-5863 (H. Yang)

Abstract

Sb-doped SnO_2 (ATO) powders were favorably synthesized using a dual-titration co-precipitation method for the application of energy-efficient windows. A dual-titration co-precipitation method can effectively inhibit the aggregation of primary nanoparticles, which is conducive to prepare stable dispersion applied to glazing materials for blocking part of solar radiation. Various annealing temperatures, doping molar ratios and ethanol content of precursor solution were used to investigate the influence on the morphology and phase composition of the as-synthesized ATO powders. The results illustrated that the reasonable reaction conditions to prepare ATO powders with near-infrared shielding property should be: the doping molar ratio of 10%, the content of ethanol in precursor solution of 100% and the annealing temperature of 1000℃. Besides, ATO primary nanoparticles were gained ranging from 45 to 55nm with a low aggregated degree. The ATO coating prepared by the ATO dispersion with 20 wt% demonstrated the optimal selective transmitted spectra, which simultaneously achieved the average visible transmittance of 80.15% but average near-infrared

transmittance of 23.31%. In addition, a simulated experiment demonstrated that ATO coated glass exhibited a better near-infrared shielding property than ITO (Sn-doped In_2O_3) coated glass.

Keywords: Sb-doped SnO_2; dual-titration co-precipitation; low aggregated degree; near-infrared shielding property; energy-efficient windows

1. Introduction

Increasing energy consumption with substantial emission of greenhouse has consumed a lot of fossil energy and caused climate change. It was reported that the energy consumption in building sectors constituted 20.1% of the overall energy consumption worldwide, which was even higher than 40% in the United States [1-3]. The electricity consumed by heating, ventilating and air conditioning constitute a high proportion of the total building energy consumption [4]. Solar heat shielding techniques and passive cooling technology are becoming more widely used for energy saving and energy crisis prevention [5]. Glazing materials, a necessary component of buildings, can increase energy consumption easily [6]. Owing to the high U values and transparency of glazing materials, the electricity consumption on air-conditioning systems is high in the summers, which results in high greenhouse gas emission. Therefore, some studies have been conducted on the development of transparent solar heat shielding materials for building windows [7, 8].

Transparent conductive oxides (TCO) significantly affect various optoelectronic devices because of their high optical transparency and good electronic conductivity [9]. In general, typical transparent conductive oxides can be doped with some elements to improve the free charge carrier concentration [10]. Hitherto, Sn-doped In_2O_3 (ITO) remains the most widely used functional filler for near-infrared shielding. However, indium is a rare metal thatis not cost-effective for commercially scalable production. Hence, non-toxic and inexpensive alternatives such as Sb-doped

SnO_2 (ATO) are desirable [11]. Doped antimony can endow tin oxide with more free electrons in the crystalline structure [12], which enables high visible transmittance and solar heat shielding performance because of localized surface plasmon resonance (LSPR) [13]. Currently, ATO powders have been successfully prepared by the following methods, sol-gel [14, 15], metalorganic deposition [16], magnetron sputtering [17], pyrolysis [18, 19] and chemical co-precipitation [12, 20]. Among these methods, co-precipitation is considered as a scalable method to synthesize ATO powders with near-infrared shielding property because of the short synthesized time required, low material cost and large-scale production potential [21]. Even though this method can yield a considerable amount of ATO powders within a reasonable cost, it is still difficult to synthesize primary particles with a low aggregated degree, which is not conducive to the subsequent dispersion processing. This is because ATO powders synthesized by the traditional co-precipitation method are easier to aggregate in the precursor solution. Specifically, a precipitant is added dropwise to a solution containing large quantity of Sn^{4+} and Sb^{3+} ions, which can accelerate the hydrolysis reaction to initiate aggregation. Aggregated particles are detrimental to the visible transmittance, because they impose a strong scattering effect to incident light [22]. Here, a dual-titration co-precipitation method is presented for the synthesis of ATO nanoparticles with high near-infrared shielding property. Crystalline nucleation and growth occur in the mixed solution of ethanol and deionized water instead of the solution containing Sn^{4+} and Sb^{3+} ions, which can effectively inhibit the aggregated degree of primary particles. Dual-titration can retain the Sn^{4+} and Sb^{3+} ions in the precursor solution at a relatively low concentration to decelerate the hydrolysis reaction and reduce collision chances between particles.

In this work, ATO powders were successfully prepared with high near-infrared shielding

performance applied in energy-efficient windows. The crystalline phase of synthesized particles was investigated by X-ray diffractometer (XRD). The optical performance of the coating samples was characterized by UV–vis–NIR Spectrophotometer. The morphology and crystalline structure were shown by transmission electron microscopy (TEM). In addition, the near-infrared shielding property was discussed using a stimulated experiment.

2. Experiment and methodology

2.1 Materials

The purchased reagents without further purification were provided by Wengjiang Chemistry, Guangzhou: tin chloride pentahydrate ($SnCl_4 \cdot 5H_2O$, AR), anhydrous ethanol (C_2H_5OH, AR), ammonium hydroxide solution ($NH_3 \cdot H_2O$ 25%-28%, AR), antimony chloride ($SbCl_3$, AR), deionized water and Waterborne polyurethane (WPU)

2.2 Preparation of ATO powders

2.2.1 Preparing compound solutions

ATO particles with a changing Sb-doped content were synthesized via the dual-titration co-precipitation method. For clarity, the antimony content was named as ATO-*x*, where *x* represented Sb / (Sb + Sn) (mol%). For a typical synthesized process, ATO-10 was prepared as an instance: 1.1 g $SbCl_3$ and 14 g of $SnCl_4 \cdot 5H_2O$ were mixed in the suitable anhydrous ethanol. To investigate the optimal reaction parameters and ensure the appropriate doped amount of antimony element, ATO were synthesized with various Sb / (Sb + Sn) (mol%) of 4%, 7%, 10%, 13% and 16% respectively. The influence of various ethanol concentration (volume ratios of 0%, 25%, 50%, 75% and 100%) in the precursor solution on the crystal structure of the prepared particles was examined.

2.2.2 Dual-titration method

In this work, two separating funnels were employed to load the Sn^{4+}/Sb^{3+} solution and $NH_3 \cdot H_2O$ precipitant respectively. The liquid in the two separatory funnels was simultaneously dropped into the flask below, while the blades of the mixer in the flask were stirred as shown in Fig. 1. The precipitate was formed in the flask filled with precursor solution. The dual-titration process was controlled within 1 hour. After the titration process, the resultant precursor was put in a water bath device and heated at 60℃ for 2 hours. The precursor continued to be centrifugated and rinsed three times with ethanol. The obtained ATO precursor was dried at 80℃ for 12 hours. Then, the dried precipitate was polished into powders.

2.2.3 Annealing dried powders

The obtained powders were placed in crucibles and then sintered at 1000℃ for 4 hours. After the calcination process, the obtained powders were collected for further characterization.

2.2.4 Preparation of ATO coatings on glass

The method has been presented in the reported research [12]. To prepare a stable ATO dispersion, the as-synthesized ATO particles were added into deionized water then ball-milling for 4 hours. The bead diameter chosen in this work was 1 mm. Polyvinyl alcohol (PVA) was used as the dispersant and its concentration of ATO dispersion was 2.5 wt%. After the ball-milling process, an appropriate amount of Waterborne polyurethane (WPU) was added into the ATO dispersion. Then, the mixed solution was agitated continuously at 85℃ for 15 minutes. At last, the ATO coatings were casted on the glass samples using spin-coating and then dried at 60℃ for 2 hours.

2.3 Characterization of ATO powders

The crystalline structure of the ATO particles were investigated on an X-ray diffraction (XRD) analysis (40kV, 30mA) equipped with graphite-monochromatized CuKα (λ = 0.154056 nm) and 2θ

scanning angle ranging from 20° to 80°. The morphology and composition of the synthesized powders was observed by transmission electron microscopy (TEM JEM-2010F, 200kV) equipped with a Bruker Quantax 400 EDS (energy-dispersive X-ray spectrometer) system. The UV-vis-NIR transmittance of prepared coatings was performed on Hitachi UH4150, which was in the range of 250nm-3000nm.

2.4 Near-infrared shielding property

Fig.2 shows the test devices for the near-infrared shielding performance. The test was carried out at a room temperature of 21.23℃. A halogen lamp of 50W was employed as the irradiated source. The top of the airtight container was covered using the different glass samples as shown in the diagram, and then the inside temperature of the sealed box was recorded in the real time using the inserted electronic thermocouple. It is noted that the probe of thermocouple shouldn't be straight illuminated by halogen lights aiming to avoid measurement errors.

3. Results and discussion

3.1 The effect of the reaction conditions on the synthesis of ATO powders

3.1.1 The influence of Sb-doped content on crystalline structure

Fig. 3 illustrates the XRD patterns of synthesized ATO powders with different Sb-doped content after sintering at 1000 ℃. The standard XRD pattern of Cassiterite SnO_2 (JCPDS 41-1445) was exhibited below the sample ATO-4. The XRD patterns of ATO-4, ATO-7 and ATO-10 exhibited the identical crystalline phase, implying that they were of a single-phase without any other crystalline phase. The existence of SnO_2 crystalline structure demonstrated that Sb ions replaced Sn ions in the crystal lattice of SnO_2. As for ATO-13 and ATO-16, some unknown characteristic peaks were observed between two peaks which corresponded to lattice planes (110) and (101), implying

that other crystalline phases appeared.

Moreover, the crystallite size was roughly calculated via the Scherrer formula [23] shown in equation (1).

$$D = \frac{K\gamma}{\mathrm{B}\cos\theta} \qquad (1)$$

Here, D represents the calculated crystallite size; *K* indicates the Scherrer constant 0.89; B denotes the full wave at half maximum also known as FWHM; γ refers to the wavelength of X-ray (0.154056nm) and θ is the half of the scanning angle. The average crystallite size was calculated based on FWHM of the strong characteristic peaks shown in Fig. 3 and results are shown in Table 1.

In Table 1, the crystallite size changes from 27.8 to 43.5 nm. It can be attributed to the tangible that Sn^{4+} ions are larger than Sb^{5+} ions (radius of Sb^{5+}: 0.60 Å, radius of Sn^{4+}: 0.69 Å). Therefore, the Sb^{5+} ions can easily enter the lattice to substitute Sn^{4+} ions. Additionally, with increasing Sb-doped content, the grain sizes of (110), (101) and (211) crystal planes calculated by Scherrer's formula illustrate an increasing trend that subsenquently decreases. This could be because Sb^{3+} ions (radius of Sb^{3+}: 0.76 Å) constituted a higher ratio of the total Sb ions at a low doping amount of Sb. After reaching a critical Sb doping concentration, the Sb^{5+} ions constituted a higher proportion of the total Sb ions, which reduced the lattice space. With a further increase in the doping amount of Sb, the Sb^{3+} ions once again dominated the ratio of Sb ions. Among the five samples, it can be inferred that ATO-10 contained a relatively high level of Sb^{5+} ions, which implied more free charge carriers.

3.1.2 The influence of the ethanol content on crystalline formation

To study the influence of the precursor solution on crystalline phase, the ATO-10 powders were

prepared by a mixed solution with various ethanol concentration.

As shown in Fig. 4, all the prepared samples illustrated the lattice planes of (110), (101) and (211), indicating the samples formed the same tetragonal rutile structure. With an increase in ethanol content, the XRD pattens of the synthesized samples showed the same crystalline structure as that of the standard reference sample, implying that water or ethanol can facilitate the formation of the SnO_2 crystalline structure without any distinction. Moreover, the utilization of ethanol can weaken the aggregation extent during the drying process, which can be attributed to the formed ethoxide groups surrounding the surface of the particles. Furthermore, the ATO powders prepared by a precursor solution composed of ethanol can lead to a lower level of aggregations than other samples owing to its lower solvent polarity.

3.1.3 The effect of the annealing temperature

As shown in Fig. 5, ATO-10 precursors were sintered at 600℃, 800℃,1000℃ and 1100℃ for 4 hours respectively.

It can be seen that the XRD pattern of uncalcined ATO-10 maintained amorphous state. After calcination at 600℃, the characteristic peaks corresponding to crystalline planes (110), (101), (200), (211) and (220) appeared and no other phase was observed, implying that the crystalline structure began to form at 600℃. The crystallite size of samples calcined at 800℃ and 1000℃ calculated by Scherrer's formula were smaller than that of the sample calcined at 1100℃, because the high calcination temperature would cause severe aggregation. In addition, the characteristic peak intensity of the (110) crystalline plane of each calcined sample was higher than that of (101), which was also reported in a previous study [24].

Fig.6 shows the images of ATO-10 precursors before and after annealing at various temperature.

It can be seen that the powders color before calcination appeared grayish yellow. With the increase in the calcination temperature, the color of the synthesized powders changed from dark gray to blue. This transition can be ascribed to the increase in Sb^{5+} ions in the crystalline lattice with the increase in annealing temperature. As the concentration of Sb^{5+} ions increased, more free electrons were generated and entered the conductive band, which allowed the samples to absorb the visible light of the corresponding wavelength and appear blue. However, when the calcination temperature was 1100℃, the color of the powder was lighter than the sample calcined at 1000℃, owing to the decreased concentration of Sb^{5+} ions.

3.2 Morphological characterization

The morphology and EDS pattern of as-synthesized ATO-7 powders using the precursor solutions composed of ethanol and deionized water with various volume ratios were investigated by TEM (Fig. 7). It is noteworthy that the ATO-7 nanoparticles were of spherical nanoparticles with different degrees of aggregation, and the aggregated degree increased with the reduction in ethanol content. When 100% ethanol was employed, the degree of aggregation was slight as shown in Fig. 7a. This demonstrated that a higher concentration of ethanol was conducive to the preparation of ATO-7 nanoparticles with low aggregation extent, and vice versa. As shown in Fig.7f, the element composition shown in the EDS pattern exhibited the presence of O, Sn and Sb in ATO-7 and the atomic ratio of Sb/Sn was 0.069.

To further study the morphology and crystalline structure of ATO-7 nanoparticles, HRTEM was employed to characterize the prepared samples. In Fig. 8a and 8b, the HRTEM images and SAED pattern of ATO-7 powders synthesized by an ethanol precursor without deionized water indicated that ATO-7 powders comprised nanocrystals and primary particle size ranged from 45 to 55nm. In

Fig. 8c, the lattice fringes of ATO-7 illustrated that the preferential growth directions were [110], [101] and [200]. The spacing calculated by the FFT function between adjacent lattices were 0.33455nm, 0.2549nm and 0.2319nm as shown in Fig. 8c. The diffraction rings shown in the SAED pattern corresponded to (110), (101), (200), (211) and (220) planes separately, implying that the XRD patterns agreed well with the TEM images.

3.3 Optical performance of ATO coatings

It is well known that the spectrum containing most of the solar energy is from ultraviolet light, visible light and near-infrared light, corresponding the wavelength of 280-380nm, 400-780nm and 780-2500nm respectively. Among the above types of light, near-infrared light is the main heat source [25]. ATO is widely known as a kind of typical transparent conductive oxides, which shows a strong near-infrared shielding property owing to its localized surface plasmon resonance [26].

To obtain the optimal near-infrared shielding performance at different wavelength, the effect of ATO dispersions of different solid content on optical property was investigated. Fig. 9 shows the transmittance spectra of coatings casted by ATO dispersions with different weight ratio of ATO powders (10 wt%, 15 wt%, 20 wt% and 25 wt%). It should be noted that the ATO coating illustrated an excellent shielding performance of near-infrared light ranging from 1500 to 2500nm and relatively high visible light transmittance. Among the prepared ATO coating samples with different solid contents, the solid content of 20 wt% demonstrated the optimal selective transmitted spectra whose average visible transmittance was 80.15% but average near-infrared transmittance was 23.31%.

3.4 Stimulated experiment for shielding property of coatings

For the purpose of studying the near-infrared shielding performance of the ATO coating from the

standpoint of practical application, a simulated experiment was conducted by irradiating with a halogen lamp of 50W the airtight containers equipped with the quartz glass, the ATO glass sample and the ITO glass sample, aiming to measuring the temperature response to the irradiation time. The ambient temperature during the measurement was 21.23℃.

ITO is widely used as a near-infrared shielding material in our daily life [27, 28]. Hence, ITO glass was chosen as a control. Fig. 10 shows the temperature variation of the three samples under different illumination time by a halogen lamp. The inside temperature of the airtight container equipped with the general quartz glass and ITO glass irradiated for 60 min increased to 33.81℃ and 31.59℃ respectively. By contrast, the inside temperature of the sealed container covered by the ATO glass only increased from 21.23℃ to 28.92℃. The temperature increase of the ATO glass sample was 7.69℃ and that of the ITO glass sample was 10.36℃. Therefore, the ATO glass sample illustrated a better near-infrared shielding property than the ITO glass sample.

4. Conclusions

We have favorably synthesized the ATO powders with near-infrared shielding property using a dual-titration co-precipitation method. It has been proved that the dual-titration way is conducive to inhibit the aggregation of primary particles. The optimal experimental reaction conditions to synthesize ATO nanoparticles with near-infrared shielding performance show that the molar ratio is 10% and the annealing temperature is 1000℃. The ATO coating with solid content of 20 wt% shows average near-infrared transmittance of 23.31%. Compared with ITO coated glass and common quartz glass, ATO coated glass shows better solar heat shielding performance as the coating can block nearly 76% near-infrared radiation, which demonstrates its practical value for the application in energy-efficient windows.

Acknowledgements

This work was supported by the TCS project of the Hong Kong Innovation and Technology Fund (UIT/139) and Sola Green Technologies Limited.

References

[1] Nakamura C, Manabe K, Tenjimbayashi M, Tokura Y, Kyung KH, Shiratori S. Heat-Shielding and Self-Cleaning Smart Windows: Near-Infrared Reflective Photonic Crystals with Self-Healing Omniphobicity via Layer-by-Layer Self-Assembly. ACS Appl Mater Interfaces. 2018;10:22731-8.

[2] Xu X, Zhang W, Hu Y, Wang Y, Lu L, Wang S. Preparation and overall energy performance assessment of wide waveband two-component transparent NIR shielding coatings. Solar Energy Materials and Solar Cells. 2017;168:119-29.

[3] Lee HY, Cai Y, Bi S, Liang YN, Song Y, Hu XM. A Dual-Responsive Nanocomposite toward Climate-Adaptable Solar Modulation for Energy-Saving Smart Windows. ACS Appl Mater Interfaces. 2017;9:6054-63.

[4] Mirrahimi S, Mohamed MF, Haw LC, Ibrahim NLN, Yusoff WFM, Aflaki A. The effect of building envelope on the thermal comfort and energy saving for high-rise buildings in hot–humid climate. Renewable and Sustainable Energy Reviews. 2016;53:1508-19.

[5] Zheng L, Xiong T, Shah KW. Transparent nanomaterial-based solar cool coatings: Synthesis, morphologies and applications. Solar Energy. 2019;193:837-58.

[6] Liu J, Xu Q, Shi F, Liu S, Luo J, Bao L, et al. Dispersion of Cs0.33WO3 particles for preparing its coatings with higher near infrared shielding properties. Applied Surface Science. 2014;309:175-80.

[7] Han K, Kim JH. Reflectance modulation of transparent multilayer thin films for energy efficient window applications. Materials Letters. 2011;65:2466-9.

[8] Chiba K, Takahashi T, Kageyama T, Oda H. Low-emissivity coating of amorphous diamond-like carbon/Ag-alloy multilayer on glass. Applied Surface Science. 2005;246:48-51.

[9] Pasquarelli RM, Ginley DS, O'Hayre R. Solution processing of transparent conductors: from flask to film. Chem Soc Rev. 2011;40:5406-41.

[10] Comin A, Manna L. New materials for tunable plasmonic colloidal nanocrystals. Chem Soc Rev. 2014;43:3957-75.

[11] Li Y, Liu J, Liang J, Yu X, Li D. Tunable solar-heat shielding property of transparent films based on mesoporous Sb-doped SnO(2) microspheres. ACS Appl Mater Interfaces. 2015;7:6574-83.

[12] Li Y, Wang J, Feng B, Duan K, Weng J. Synthesis and characterization of antimony-doped tin oxide (ATO) nanoparticles with high conductivity using a facile ammonia-diffusion co-precipitation method. Journal of Alloys and Compounds. 2015;634:37-42.

[13] Peters K, Zeller P, Stefanic G, Skoromets V, Němec H, Kužel P, et al. Water-Dispersible Small Monodisperse Electrically Conducting Antimony Doped Tin Oxide Nanoparticles. Chemistry of Materials. 2015;27:1090-9.

[14] Floriano EA, Scalvi LVA, Sambrano JR, de Andrade A. Decay of photo-induced conductivity in Sb-doped SnO2 thin films, using monochromatic light of about bandgap energy. Applied Surface Science. 2013;267:164-8.

[15] Dua L, Biswas PK. Synthesis and photoluminescence property of nanostructured sol–gel antimony tin oxide film on silica glass. Chemical Physics Letters. 2013;572:66-72.

[16] Feng X, Ma J, Yang F, Ji F, Zong F, Luan C, et al. Structural and photoluminescence properties of single crystalline SnO2:In films deposited on α-Al2O3 (0001) by MOCVD. Journal of Crystal Growth. 2008;310:3718-21.

[17] Zheng M, Ni J, Liang F, Wang M-C, Zhao X. Effect of annealing temperature on the crystalline structure, growth behaviour and properties of SnO2:Sb thin films prepared by radio frequency (RF)-magnetron sputtering. Journal of Alloys and Compounds. 2016;663:371-8.

[18] Lee S-Y, Park B-O. Structural, electrical and optical characteristics of SnO2:Sb thin films by ultrasonic spray pyrolysis. Thin Solid Films. 2006;510:154-8.

[19] Elangovan E, Ramamurthi K. A study on low cost-high conducting fluorine and antimony-doped tin oxide thin films. Applied Surface Science. 2005;249:183-96.

[20] Liu S-m, Ding W-y, Chai W-p. Influence of Sb doping on crystal structure and electrical property of SnO2 nanoparticles prepared by chemical coprecipitation. Physica B: Condensed Matter. 2011;406:2303-7.

[21] Chen X, Lu T, Wei N, Lu Z, Zhang W, Ma B, et al. Corrigendum to “Effect of ball-milling granulation with PVB adhesive on the sinterability of co-precipitated Yb:YAG nanopowders” [J. Alloys Compd. 589 (2014) 448–454]. Journal of Alloys and Compounds. 2014;614.

[22] Zhou Y, Li N, Xin Y, Cao X, Ji S, Jin P. CsxWO3 nanoparticle-based organic polymer transparent foils: low haze, high near infrared-shielding ability and excellent photochromic stability. Journal of Materials Chemistry C. 2017;5:6251-8.

[23] Hu Y, Zhong H, Wang Y, Lu L, Yang H. TiO2/antimony-doped tin oxide: Highly water-dispersed nano composites with excellent IR insulation and super-hydrophilic property. Solar Energy Materials and Solar Cells. 2018;174:499-508.

[24] Ravichandran K, Philominathan P. Analysis of critical doping level of sprayed antimony doped tin oxide films. Journal of Materials Science: Materials in Electronics. 2010;22:158-61.

[25] Guo C, Yin S, Zhang P, Yan M, Adachi K, Chonan T, et al. Novel synthesis of homogenous CsxWO3 nanorods with excellent NIR shielding properties by a water controlled-release solvothermal process. Journal of Materials Chemistry. 2010;20.

[26] Manthiram K, Alivisatos AP. Tunable localized surface plasmon resonances in tungsten oxide nanocrystals. J Am Chem Soc. 2012;134:3995-8.

[27] Liu H, Zeng X, Kong X, Bian S, Chen J. A simple two-step method to fabricate highly transparent ITO/polymer nanocomposite films. Applied Surface Science. 2012;258:8564-9.

[28] Tao P, Viswanath A, Schadler LS, Benicewicz BC, Siegel RW. Preparation and optical properties of indium tin oxide/epoxy nanocomposites with polyglycidyl methacrylate grafted nanoparticles. ACS Appl Mater Interfaces. 2011;3:3638-45.

Table 1

The calculated crystallite size using the Scherrer formula.

Sample	ATO-4	ATO-7	ATO-10	ATO-13	ATO-16
D/nm	43.2	43.5	27.8	42.6	42.1

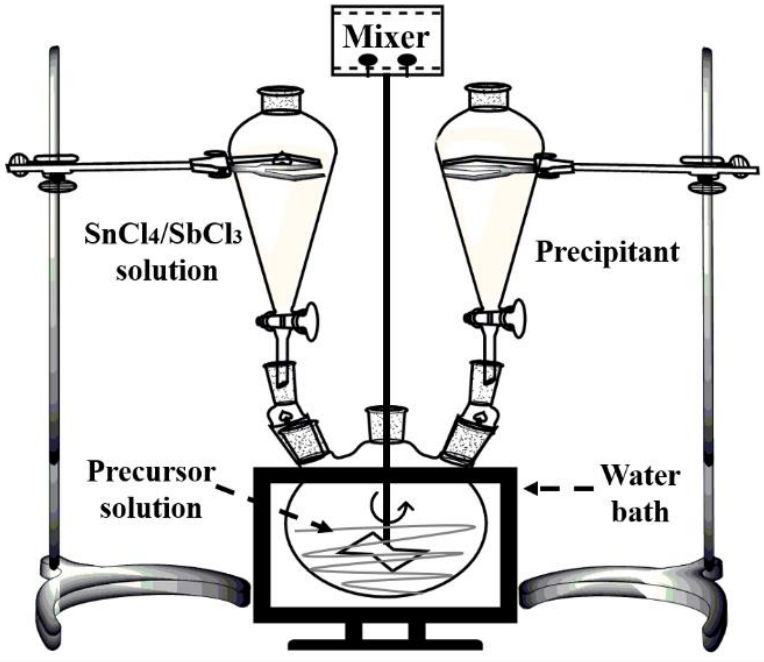

Fig. 1. Schematic illustration of the dual-titration method in the preparation process.

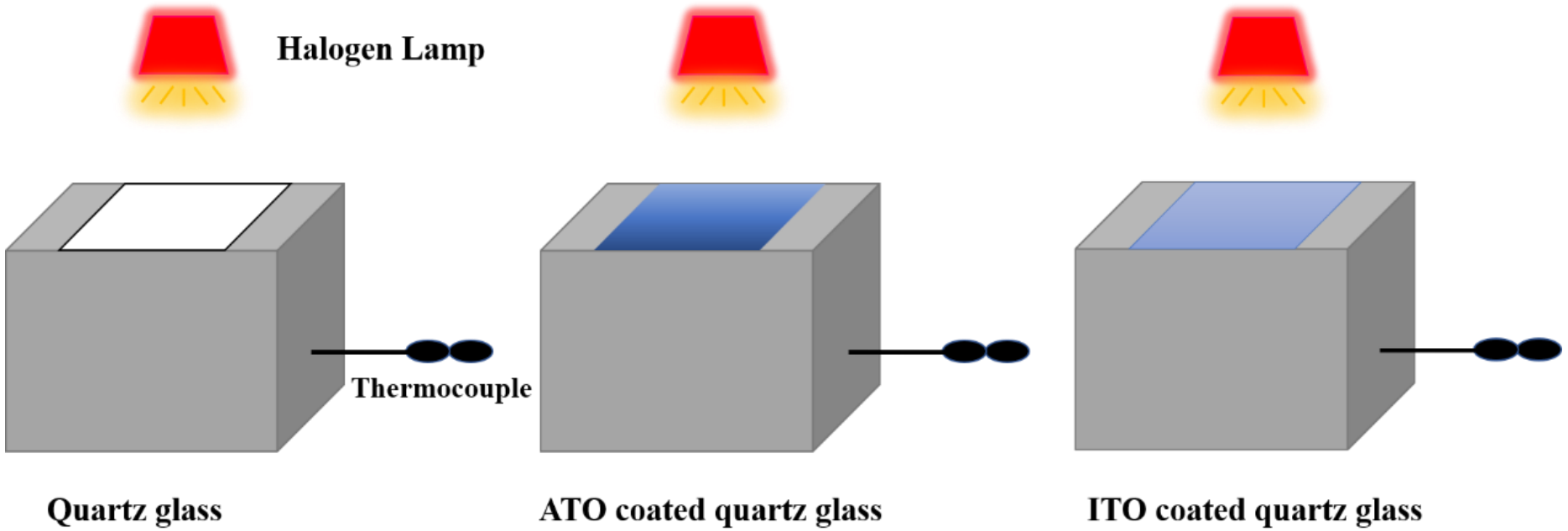

Fig. 2. Schematic diagram of the near-infrared shielding performance test.

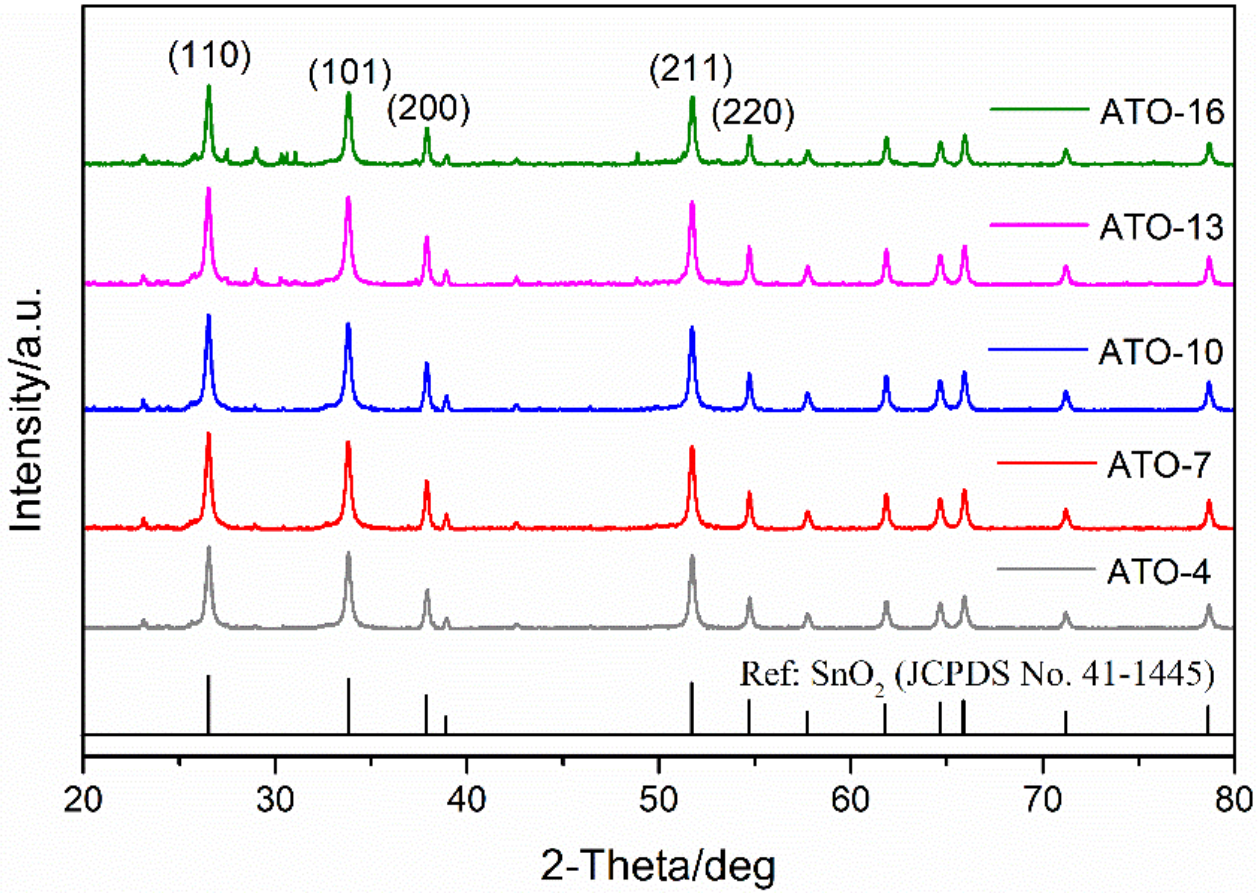

Fig. 3. XRD patterns of ATO powders with various Sb-doped content.

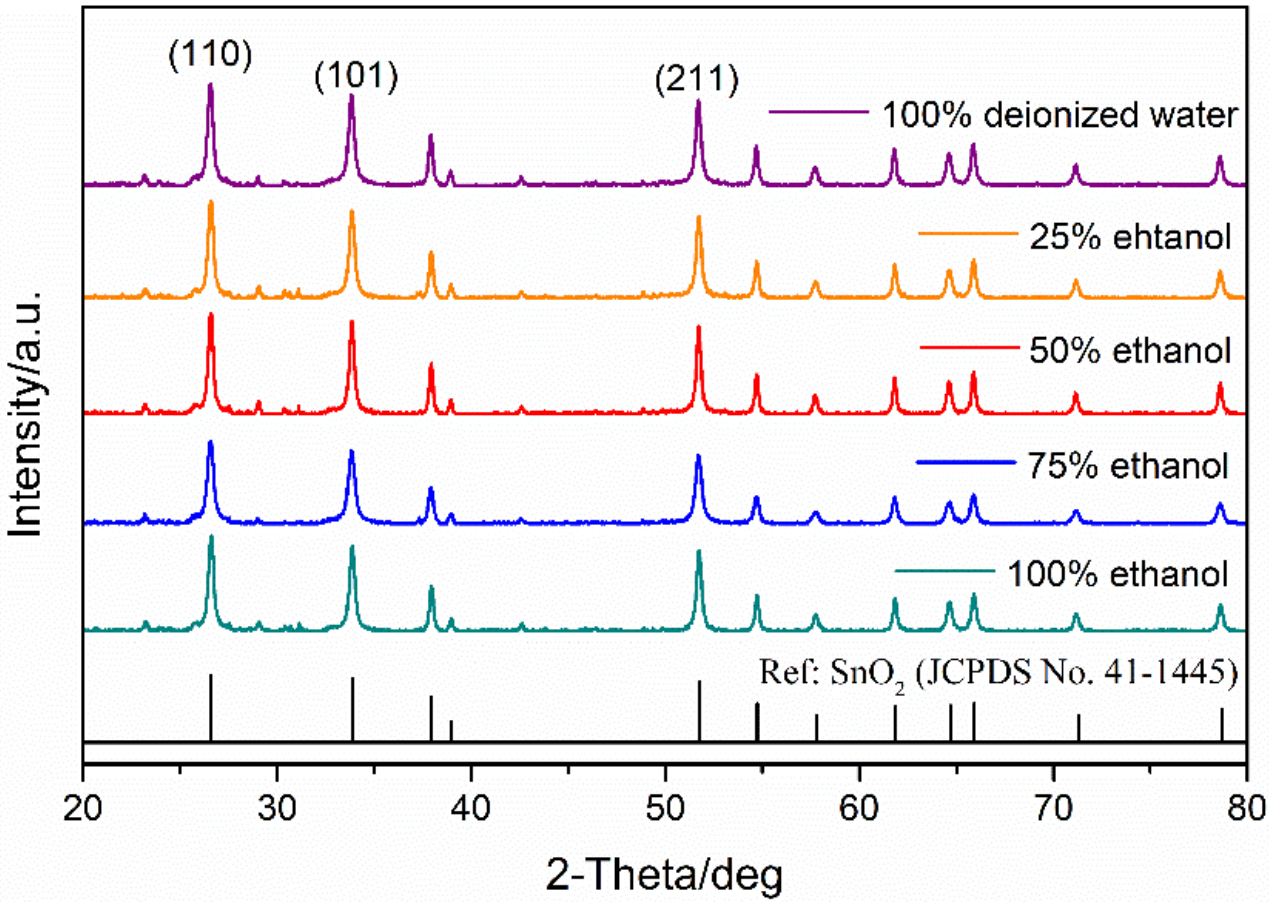

Fig. 4. XRD patterns of ATO-10 powders synthesized by precursor solution composed by ethanol and deionized water with various volume ratios.

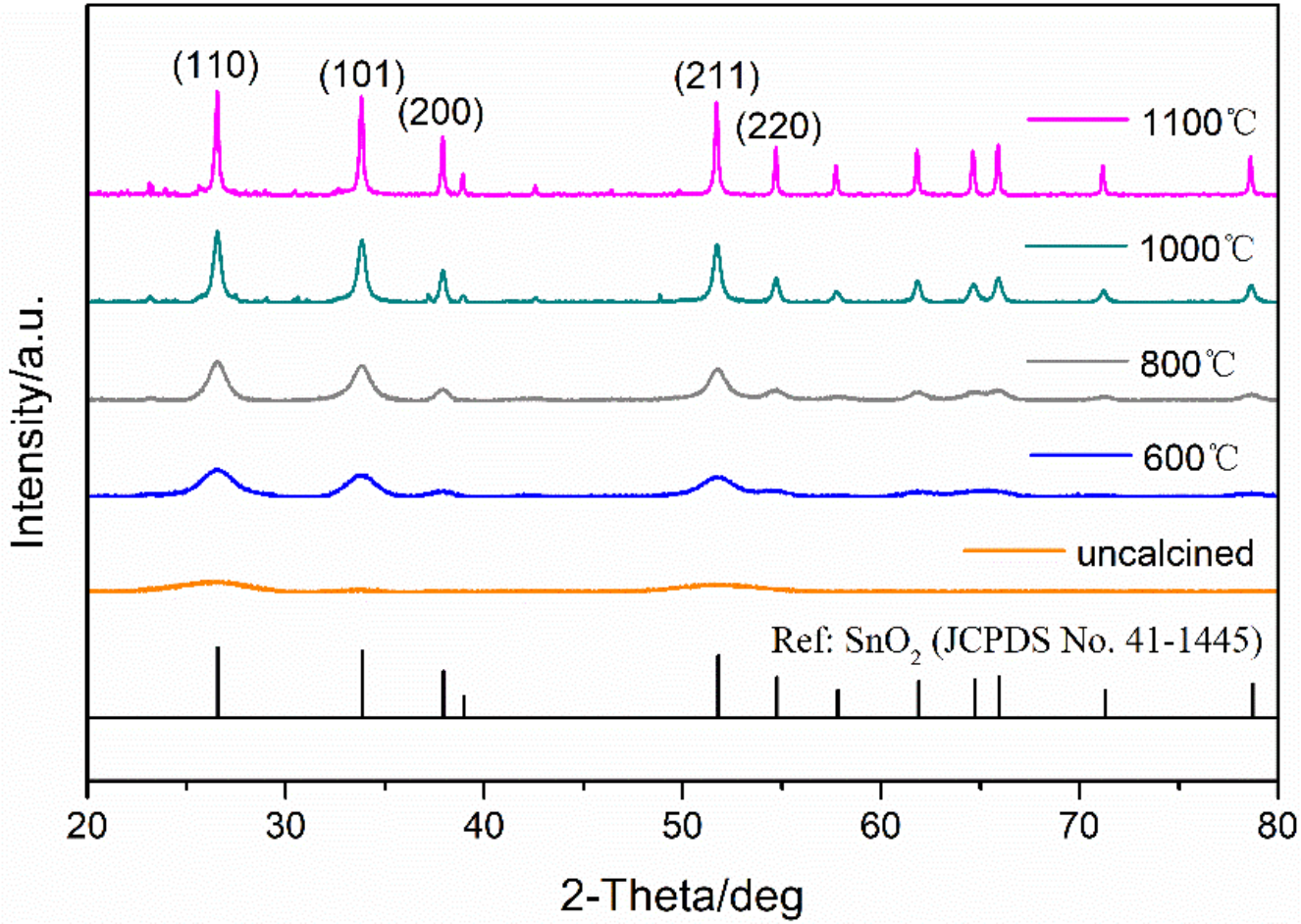

Fig. 5. XRD patterns of ATO-10 annealed at 600℃, 800℃, 1000℃ and 1100℃.

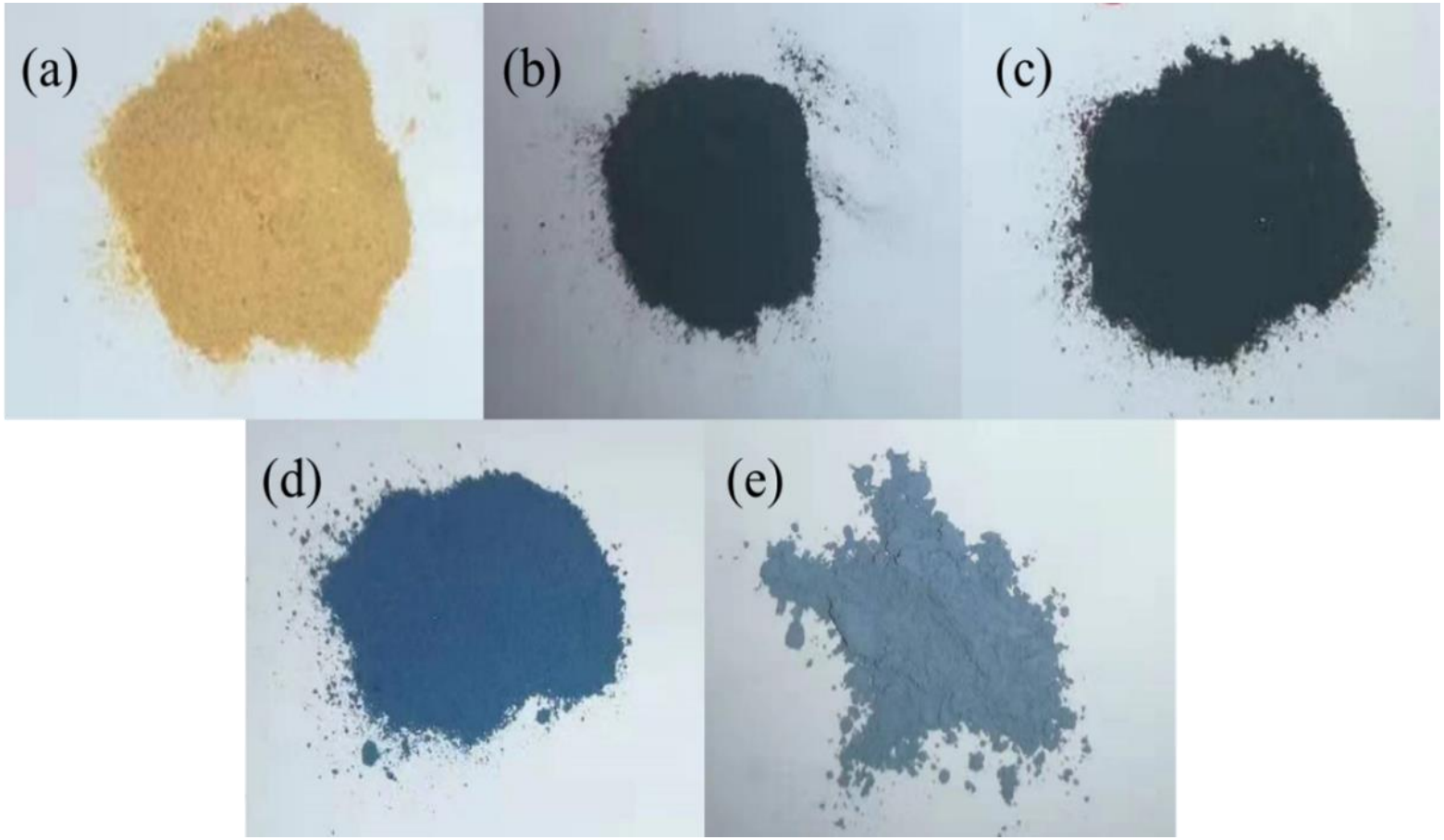

Fig. 6. The images of ATO-10 precursors (a) before annealing, calcined at (b) 600℃, (c) 800℃, (d) 1000℃, and (d) 1100℃.

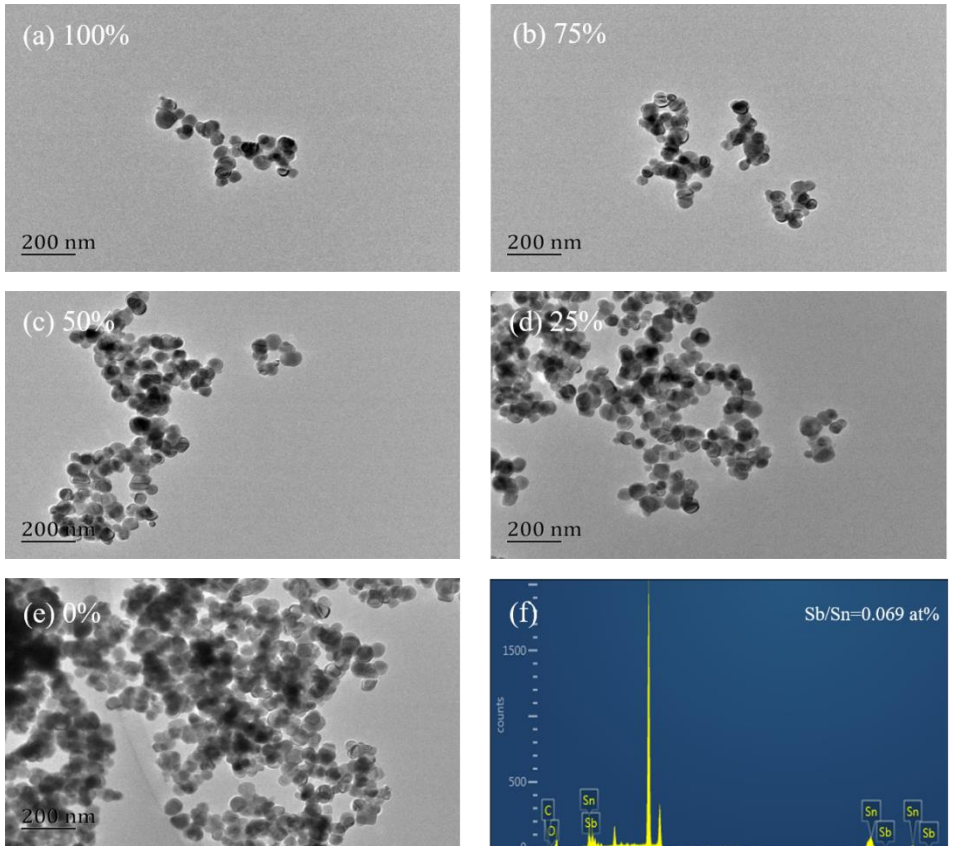

Fig. 7. TEM images of the ATO-7 powders synthesized in precursor solution with ethanol content of (a) 100%, (b) 75%, (c) 50%, (d) 25% and (e) 0% after calcined at 1000℃; (f) EDS pattern of ATO-7 powders synthesized in precursor solution with 100% ethanol content after calcined at 1000℃.

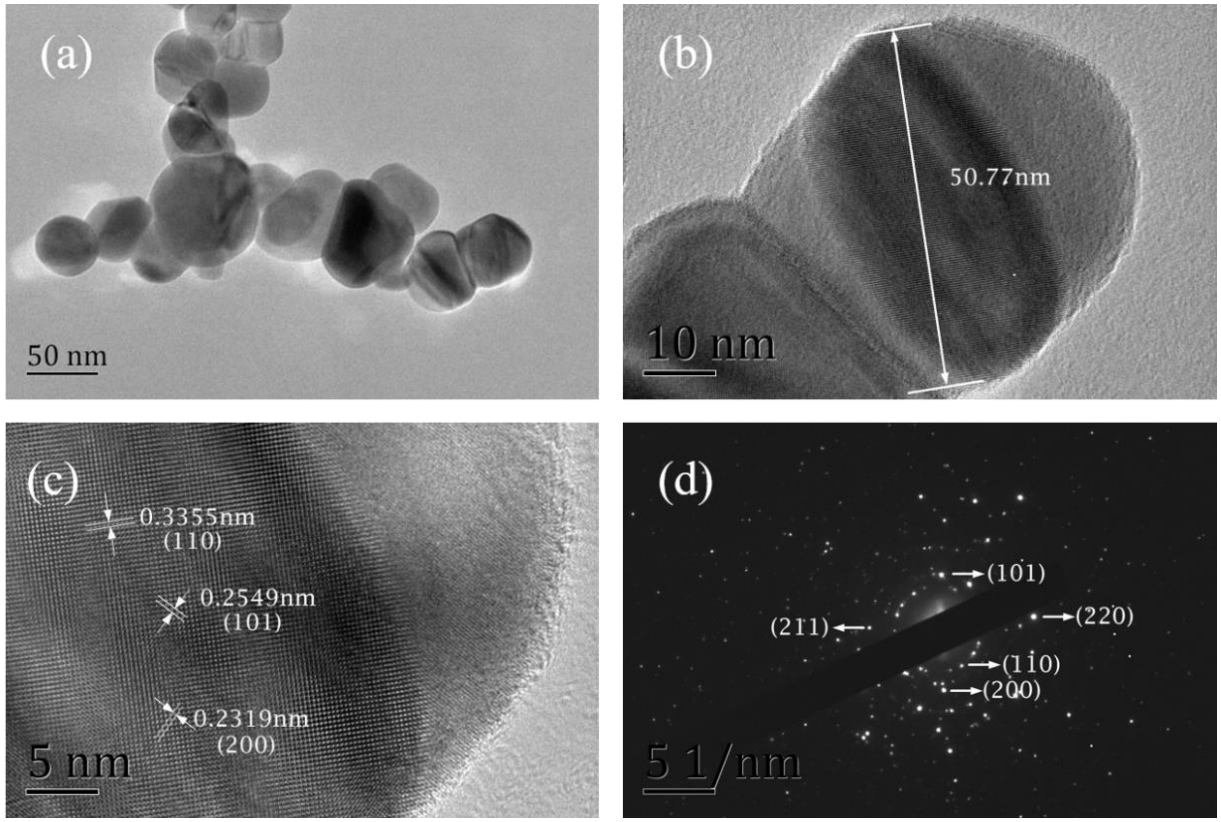

Fig. 8. (a) TEM image, (b) and (c) HRTEM images of ATO-7 powders after annealing at 1000℃, (d) SAED profile.

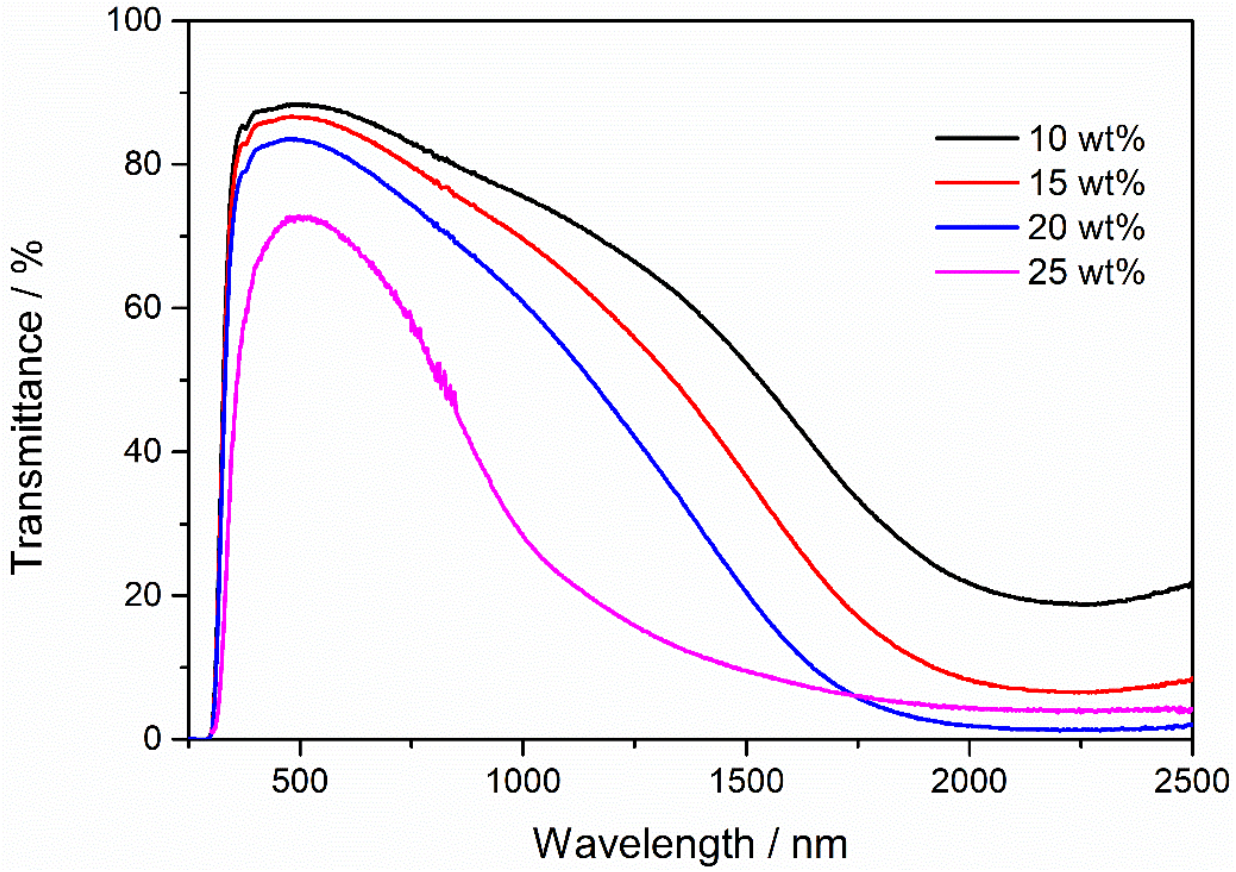

Fig. 9. Transmittance spectra of ATO coatings prepared by ATO dispersions of different solid contents.

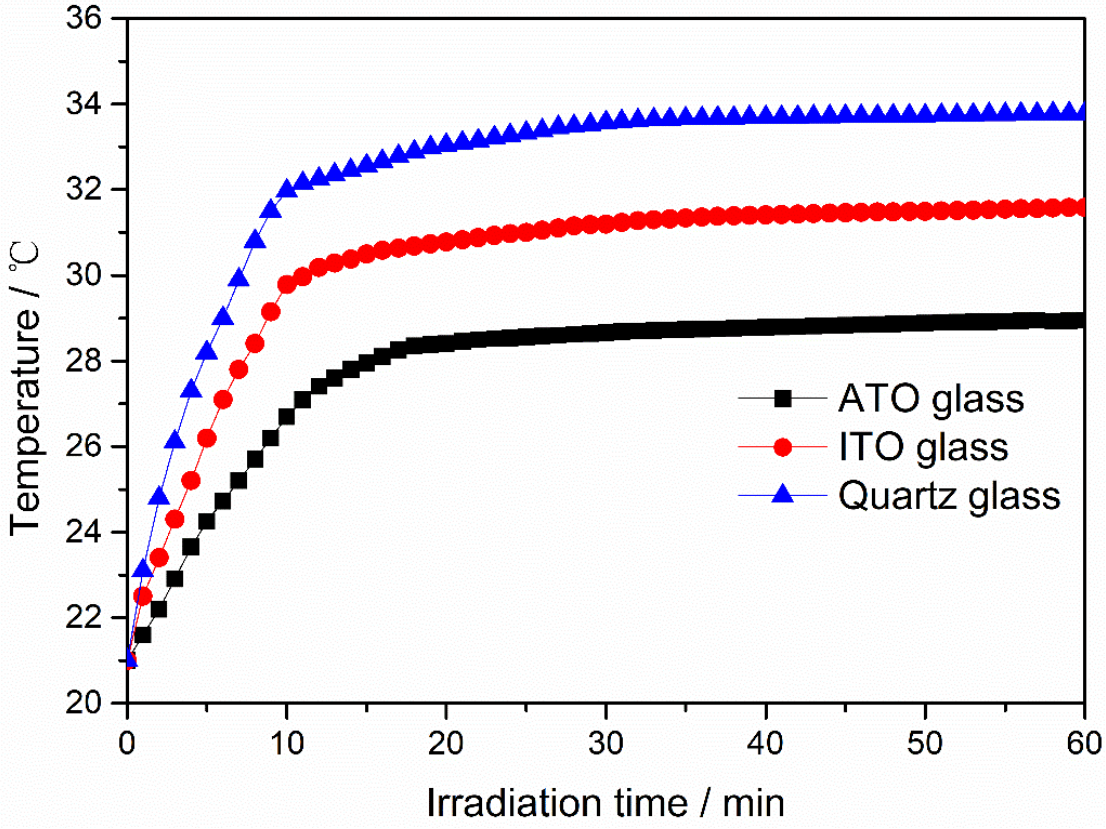

Fig. 10. The temperature variation of three glass samples with the irradiation time.